Published in final edited form as:
Anal Chem. 2008 September 1; 80(17): 6545–6553. doi:10.1021/ac800535e.

Trapping Ring Electrode Cell: A FTICR Mass Spectrometer Cell for Improved Signal-to-Noise and Resolving Power

Chad R. Weisbrod, **Nathan K. Kaiser**, **Gunnar E. Skulason**, and **James E. Bruce***
Department of Chemistry, Washington State University, Pullman, Washington 99164-4630

Abstract

A novel FTICR cell called the trapping ring electrode cell (TREC) has been conceived, simulated, developed, and tested. The performance of the TREC is compared to a closed cylindrical cell at different excited cyclotron radii. The TREC permits the ability to maintain coherent ion motion at larger initial excited cyclotron radii by decreasing the change in radial electric field with respect to *z*-axis position in the cell. This is accomplished through postexcitation modulation of the trapping potentials applied to segmented trap plates. Resolving power approaching the theoretical limit was achieved using the novel TREC technology; over 420 000 resolving power was observed on melittin $[M + 4H]^{4+}$ species when employed under modest magnetic field strength (3T) and a data acquisition duration of 13 s. A 10-fold gain in signal-to-noise ratio is demonstrated over the closed cylindrical cell optimized with common potentials on all ring electrodes. The observed frequency drift during signal acquisition over long time periods was also significantly reduced, resulting in improved resolving power.

Fourier transform ion cyclotron resonance mass spectrometry[1] (FTICR-MS) provides high resolution, mass measurement accuracy, and sensitivity which makes it ideally suited for analytical application in the areas of proteomics,[2–4] metabolomics,[5] petroleomics,[6,7] and many others. FTICR-MS is the high performance end of proteomics research today, with the capability to identify proteins and protein–protein interactions based on accurate mass measurements.[8–10] In general, the more accurately a mass can be determined, the more confident identification can be assigned for a given protein[11,12] and the more confidently unknown peptide sequences can be determined.[13] The goal to apply mass spectrometry to ever-increasingly complex biological samples furthers the demand for increased analytical capabilities and the need for development of higher performance instrumentation.

The FTICR mass spectrometer relies upon an electromagnetic ion trap or cell to confine ions during detection.[14–16] The confinement is accomplished radially (*x*–*y* dimension) by an applied magnetic field parallel to the *z*-axis of the ion trap and axially using DC electrical potentials applied to trapping electrodes. As an ion approaches either trap plate, it experiences a force due to the electric field, and its kinetic energy is converted to potential energy. Thus, the ion exhibits periodic motion similar to the classical harmonic oscillator. As a consequence of the method by which ions are trapped within the cell, four natural motions arise. Trapping oscillation is the motion in which the ions oscillate in the *z*-dimension of the cell. Cyclotron motion is caused by the Lorentz force and is dependent upon the mass-to-charge ratio (*m*/*z*) (eq 1).

*Corresponding Author. Phone: (509) 335-2116. Fax: (509) 335-8867. james_bruce@wsu.edu.

SUPPORTING INFORMATION AVAILABLE

Supplemental Figures 1–4. This material is available free of charge via the Internet at http://pubs.acs.org

$$\omega_c = \frac{qB_o}{m} = \frac{zeB_o}{m} \quad (1)$$

Where ω_c is the cyclotron frequency, z is number of charges, e is the charge of an electron, B_o is the magnetic field strength, and m is the mass. Equation 1 represents the unperturbed cyclotron frequency, which is only dependent upon the *m/z* of the ion and the magnetic field strength. Cyclotron orbital motion is detected and related back to *m/z* in FTICR-MS analysis. The third motion, magnetron motion, is caused by the radial component of the electrostatic field confining the ions in finite FTICR cells.[17] The radial electric field is perpendicular to the magnetic field and results in the $\vec{E} \times \vec{B}$ drift of the ions around the center of the ICR cell. Ion cloud rotation, the final of the four natural motions, results from the electric field generated by the ion cloud itself.[18]

Signal duration, and consequently performance, in FTICR-MS is influenced by many factors, but the two most notable are collisional damping[19] and ion-cloud dephasing.[20] Collisional damping is a signal decay process which is proportional to pressure; therefore, reducing the pressure in the cell region decreases signal decay, due to fewer collisions. Ion-cloud dephasing is thought to be caused by a culmination of effects; three of which have been heavily documented include: magnetic field inhomogeneity, electric field inhomogeneity,[21–23] and Coulombic interactions[18,24–26] occurring between ion clouds of differing *m/z*. As such, many high resolution FTICR measurements employ relatively low trapping potentials in order to minimize electric field inhomogeneity and its deleterious effect on coherent ion motion.[27,28] The use of low trapping potentials requires that the ions entering the cell have sufficiently low kinetic energy to remain confined. Collisional cooling is a method of thermalizing ion kinetic energy; however, the undesirable pump-down time required to regain the low pressure needed for measurement ($\leq 10^{-9}$ *torr*) hinders high-throughput analysis. Magnetron frequency and space charge normally both reduce the observed cyclotron frequency as illustrated in eq 2.[29]

$$\omega_{obs} = \omega_c - \omega_m - \delta \quad (2)$$

In eq 2, ω_{obs}, ω_c, ω_m, and δ are the observed cyclotron frequency, the “unperturbed” cyclotron frequency, the magnetron frequency, and the collective effect of ion–ion interactions, respectively. It should be noted that the sign of the magnetron frequency term is dependent upon the direction of the radial component of the electric field force acting on an ion.[30] Outward-directed radial fields result in magnetron motion opposed to cyclotron motion, and thus, reduce the observed cyclotron frequency.

A major limitation of current FTICR-MS instrumentation results from nonideal electric fields present within the cell.[28] Electric fields are necessary, as previously mentioned, to confine the ions in the axial dimension, but the unfortunate artifact of finite cell geometry is a radially directed component of the electric field. The radial electric fields resulting from finite Penning traps have been of concern to investigators since the initial trapped cell experiments.[15] Two main solutions to improve the electric fields have been explored: segmentation of trapping electrode surfaces[31–36] and changing the physical geometry of the cell.[37–39] Many FTICR instruments, including those produced commercially, utilize orthorhombic (cubic) and cylindrical (open and closed) cell geometries. Other geometries, such as the hyperbolic cell,[38,39] present examples in which changing the geometry of the cell can result in an exactly quadrupolar trapping potential. A quadrupolar field is advantageous for FTICR-MS because ions will exhibit a cyclotron frequency that is independent of radius. Most cell geometries approximate a quadrupolar field in a small

region near the center of the cell, but deviation from quadrupolar potential in cell geometries other than the hyperbolic cell becomes more severe as *z*-axis oscillation amplitude increases.

Segmentation of electrode surfaces is another approach utilized to regulate the electric fields within the trapping region. Gabrielse introduced the idea of using compensation electrodes to reproduce the quadrupolar field of the hyperboloid cell geometry.[40,41] Others have recently further developed this idea.[32,35] Gooden et al. produced an excite coupled cubic cell with a disk electrode centered on opposing trap plates for frequency focusing.[33] Wang and Marshall[42] showed improvements by using a trapping well shape that drops to nearly zero potential over most of the cell volume when a grounded screen is placed within a conventional orthorhombic cell. A cylindrical cell design with three pairs of circular electrodes spaced along the *z*-axis was developed by Naito et al.[43] This cell was shown to have reduced radial electric field and to have a smaller drift (magnetron) frequency when compared to the conventional open cylindrical cell.

Electric field nonideality exists during ion excitation in addition to detection. Research efforts on cell development have yielded multiple approaches to linearize the radio frequency (RF) excitation potentials through variations of the orthorhombic and cylindrical cell.[44,45] These designs reduce the problem of axial ejection of the ions due to *z*-axis excitation[46] resulting in significant improvements over their predecessors, the closed cylindrical cell and the open cell. However, inhomogeneity in the radial electric field over the trapping region at the excited cyclotron radius has not been addressed in combination with any previous design.

Our recent efforts have shown that for commercial FTICR-MS instruments, two factors that include ion *z*-axis kinetic energy spread and radial electric field variation experienced along the *z*-axis after the ions reach the excited cyclotron orbit are dominant factors that affect instrument performance during detection.[47–49] In addition, we showed that, by implementing an electron beam in the center of the cell during the detection of cyclotron motion, increased phase coherence, time-domain signals and resolution could be achieved.[47] The basis of this Electron Promoted Ion Coherence or EPIC was also shown to be the minimization of radial electric field variations encountered by ions with differing *z*-axis kinetic energies.[49] This variation in radial electric fields in a conventional ICR cell results in different magnetron frequencies for ions with differing *z*-axis kinetic energies. The distribution of *z*-axis kinetic energies translates to a spread in *z*-axis positions where ions spend a majority of the time in the cell. Because of the magnetron frequency differences, the observed cyclotron frequencies are also slightly different for these ions, and results in dephasing of ion motion due to this slight frequency difference. This dephasing mechanism is reduced with the application of EPIC due to the reduction in variation of radial fields along the *z*-axis encountered by the ions during detection of excited cyclotron motion. Building on these studies, we sought to develop an ICR cell that could also provide the ability to tune radial field components at any chosen cyclotron radius without the need for an electron beam.

A unique modification to the closed-cylindrical FTICR cell is presented in this publication. The Trapping Ring Electrode Cell, or TREC, achieved improved performance by segmentation of the trap plates into five concentric ring electrodes spatially positioned in the same plane as the original disk-like trap plate (Figure 1). These ring electrodes are independently controlled and modulated to a preset potential profile subsequent to excitation of the ions. Previously, the primary focus of ICR cell development has been the quadrupolar fit of the electric field confining ions or linearization of RF potentials. In contrast, our efforts aim to reduce the variance in the radial field component along the *z*-axis *at the excited ion cyclotron radius*. The overall quadrupolar field quality may be significantly worse than that

of a conventional ICR cell. Achieving a quadrupolar field in order to exploit the aspect that cyclotron frequency is independent of cell radius is applicable to damping of cyclotron orbit. This would provide a measurement of cyclotron frequency which would not change as a function of damping. However, the results presented here indicate that ion-cloud dephasing is instead the dominant mechanism of signal decay under the operating pressure of most ICR experiments (~10^{-9}–10^{-10} Torr). Therefore, the TREC development illustrates a previously under-recognized critical aspect of electric fields that limit ICR performance. Thus, the TREC provides a new way to achieve improved ICR performance by minimizing radial field variance encountered by ions after cyclotron excitation. Narrowing the spread in ion *z*-axis kinetic energies is difficult to achieve in the absence of ion neutral collisions, and even more so during operation of the mass spectrometer with scan rates compatible with online LC separations. The TREC provides a novel approach to performance enhancement that allows one to overcome ion kinetic energy spread and radial field limitations. These attributes will likely provide more accurate analysis at higher duty cycle.

EXPERIMENTAL SECTION

TREC Design

The conceptual illustration and schematic for the first generation TREC design was rendered using SolidWorks 2004 (SolidWorks Corp., Suresnes, France). The ring electrodes were machined from solid oxygen free high conductivity (OFHC) copper. The braces, which ensure spatial uniformity and electrical isolation of the copper rings, were machined from MACOR machinable glass ceramic (Morgan Advanced Ceramics, Fairfield, NJ). The ring width is 0.110” and the spacing between each ring is 0.039”. The thickness of the rings is 0.063”. Machining tolerances for the MACOR braces and the copper ring electrodes are ± 0.005”. Commercially pure titanium (CP-Ti) 2–56 socket cap screws (United Titanium, Wooster, OH) were used to fasten the MACOR braces to the ring electrodes and also serve as the terminals for wiring the DC potentials to the rings. All ten rings were wired separately, affording independent control over the DC potentials on each ring. Kapton coated wire (MDC Vacuum Products Corp., Hayward, CA) was used for electrical connections to the trapping ring electrodes. Tin-coated copper ring-tongue solderless connectors (McMaster-Carr, Los Angeles, CA) were used to connect the Kapton wire to the terminals on the cell. The cell had an inner diameter of 1.875” and a length of 2” between trapping electrodes. All of the materials used in the construction of the TREC were chosen with “outgassing” and magnetic field homogeneity as primary concerns.

TREC Operation

Generation of independently variable DC voltages for each of the ring electrodes was accomplished using a program developed in-house within LabVIEW 8.0. The process occurs through two computers working in concert, a MIDAS[50] data station and a computer housing the National Instruments hardware. Analog voltages are read in and digitized from the MIDAS data station through a NI board (NI PCI-6111, National Instruments, Austin, TX). These voltages are then supplied to all ten ring electrodes through another NI board (NI PCI-6723, National Instruments, Austin, TX) during all FTICR experimental events in which static or common potentials are applied. For the detection period, or any other period in which custom trap potential profiles are desired, the trapping rings are modulated to values (−10 to +10 V) preset by the operator in the LabVIEW program. Switching from TREC to static (non-TREC) conditions is done using a transistor-transistor logic (TTL) trigger pulse from the MIDAS to the hardware computer. The variability in the switching times was observed using an oscilloscope and on average was ± 25 μs. This “jitter” in the time for voltage switching is negligible with respect to the detection interval and was acceptable for our experiments. From this point forth, non-TREC conditions (common

conditions) will be defined as all rings having the same voltage applied during detection. TREC conditions will be defined as the modulated case in which the voltages are switched to a preset scheme during detection. Voltages will be listed in the order from smallest to largest ring electrode radius. For example, (0.2, 1.1, 1.6, 2.4, 2.8 V) will indicate the DC voltages applied to the five rings composing the front and rear trap plates from smallest to largest radius, respectively.

SIMION Modeling

Modeling of the TREC was performed using SIMION 3D version 7.0 (D. A. Dahl, Idaho National Engineering and Environmental Laboratory). The model was designed to scale with the actual TREC design using 0.25 mm/grid unit and refined to a convergence level of 10^{-5}. Equipotential contour plots illustrate the approximate potentials within the cell during experiments with static or common voltages on all rings for both non-TREC and TREC conditions. Radial electric field plots were generated by recording the electric field component in the y-direction on an ion at millimeter increments across the cell at a given radius for both non-TREC and TREC conditions (~38% cell radius).

FTICR-MS Experimental Conditions

The spectra presented here were obtained from a constructed-in-house 3.0 T Fourier transform ion cyclotron resonance mass spectrometer. This novel instrument will be discussed in a forthcoming publication,[51] therefore, only the features relevant to the present data will be mentioned here. Electrospray ionization (ESI) was used as the source for all spectra presented. Ions were accumulated in a region of higher pressure in a quadrupole, then transferred to the cell via a set of RF-only quadrupoles. Spray solutions were composed of 49% ultrapure water (18 MΩ), 49% methanol (HPLC grade), and 2% acetic acid. Analyte concentrations for bradykinin, melittin, and ubiquitin (Sigma-Aldrich, St. Louis, MO) were 10 μM in spray buffer for all experiments. The ESI flow rate for all FTICR experiments was 1 μL/min. The potential on the ESI probe was defined as 2.5 kV and the flared capillary inlet[52] was placed at 200 V. The pressure in the cell region during all experiments was approximately 5×10^{-9} Torr.

In single scan experiments, ion cooling was accomplished by pulsing argon gas into the cell region for 1 ms followed by a 10 s pumping delay to remove excess neutrals prior to excitation. In experiments with common 1.1 V detection conditions, frequency swept excitation ranging from 20 to 220 kHz with an amplitude of ~31 V_{p-p} was used to induce coherent cyclotron motion of the melittin ions. For the common 2.0 V detection conditions and TREC conditions (0.2, 1.1, 2.0, 2.4, and 2.8 V), frequency swept excitation ranging 20 kHz to 220 kHz with an amplitude of ~40 V_{p-p} was used to induce coherent cyclotron motion of the melittin ions. The spectra shown were acquired at a sample rate of 160 kHz/s; 8 Megapoints of data were collected for each spectrum.

Radial dependence of signal intensity and S/N ratio of detected FTICR signals were investigated with single frequency excitation of bradykinin $[M + 2H]^{2+}$ ions. Gated trapping was used to confine ion populations within the cell. A frequency of 87.4 kHz was applied for a total of 150 μs to induce coherent cyclotron motion of the ions. 64 K datapoints were collected at 160 kHz/s. For the S/N characterization experiments, the excitation amplitude applied was ~20, 28, 33, and 39 V_{p-p}, corresponding to ~35, 45, 55, and 65% cell radius, respectively (calculated from single frequency version of eq 3). The voltage profiles selected for each excitation condition in the S/N characterization experiments were 35% (0.9, 1.0, 1.2, 1.6, and 2.0 V), 45% (0.8, 1.6, 2.0, 2.4, and 2.8 V), 55% (0.4, 1.2, 1.6, 2.0, and 2.4 V), and 65% (0.2, 0.8, 1.6, 2.0, and 2.4 V). Accumulation time was varied for each excitation condition from 0.1 to 1 s. For the investigation of radial dependence on the signal intensity,

the following voltage profiles were applied to the trapping rings during detection: TREC 1 (0.8, 1.6, 2.0, 2.4, 2.8 V), TREC 2 (0.2, 0.8, 1.6, 2.0, 2.4 V), and TREC 3 (1.2, 1.4, 1.6, 2.0, 2.4 V). The names of these voltage profiles will be referred to without mention of the actual voltages henceforth for simplicity. Ion accumulation was set to 100 ms. Excitation amplitude was varied in 1.6 V_{p-p} increments.

All acquired FTICR data were analyzed with ICR-2LS.[53] The high resolution melittin data sets were subject to Fourier transform without any further processing. After the Fourier transform to the frequency domain, signals corresponding to the $[M + 4H]^{4+}$ were selected and inverse transformed to the time domain to better visualize the signal decay rate. A subsequent reverse Fourier transform was applied to obtain the time domain signal isolated for the $[M + 4H]^{4+}$ isotopic envelope.

RESULTS AND DISCUSSION

In previous studies with EPIC,[47–49] we showed an increase in FTICR-MS instrument performance. However, the observed cyclotron frequency was very sensitive to the number of electrons in the electron beam. The poor reproducibility of the number of electrons present during multiple experiments proved inadequate for analytical applications with current hardware. Therefore, we have designed an FTICR cell that has the ability to tune radial electric fields, much like we observed with EPIC. In this new design, the flexibility and reproducibility in the resultant electrostatic fields are improved compared to what we observe with EPIC. The conceptual representation of the TREC is shown in Figure 1a and 1b. A perspective view of the cell is shown in Figure 1a whereas Figure 1b is an enlargement of one segmented trap plate.

The electric field generated from a radially symmetric arrangement of electrodes is composed of an axial and a radial component. The radial component and its variation over the *z*-axis coordinates are most important to the present discussion. Experimental comparison to the closed cylindrical cell can be made to a good approximation when common voltages are applied to the rings (non-TREC conditions). Figure 2a shows the equipotential contour plots produced by applying common 2.0 V potentials to all five rings in an effort to mimic the common 2.0 V conditions produced using a standard closed cylindrical cell design. The equipotential contour plot under TREC conditions with an applied potential scheme on the rings is shown in Figure 2b. Potentials applied on each ring with increasing electrode radius are 0.2, 1.1, 2.0, 2.4, and 2.8 V, respectively. The key feature to compare between Figure 2a and b is the location in the cell where the change in radial electric field ($-dV/dr$) is minimized along the *z*-axis for either set of trapping conditions. In the case of the closed cylindrical cell, by imposing static conditions, the location where radial electric field is minimized occurs about 0% cell radius. This is good for minimizing magnetron motion at 0% cell radius, but this is not an advantageous electric field environment during detection, because ions orbit at some cyclotron radius (usually 30–50% cell radius). Decreasing the radial electric field over ion *z*-axis oscillation is important to the overall performance of the cell because any component of the electric field not directed axially within the cell results in outward directed force acting upon the ions. Additionally, the radial electric field is proportional to the contribution of magnetron frequency to the observed cyclotron frequency. From the equipotential contour plots, we have demonstrated with the TREC the ability to shift the position where the radial electric field has been minimized outward from the central axis of the cell, providing the region of decreased radial electric field at or near a given excited cyclotron radius. More importantly, this region can be tuned simply by changing the voltage modulation scheme appropriately.

The voltage modulation scheme applied to the TREC in Figure 2b was first arrived at experimentally through multiple experimental iterations where the applied voltage to one pair of ring electrodes was independently varied until an optimal value was obtained for each ring. The nonlinear DC voltage ramp was found through experiment to work well in a general sense, i.e., for all of the species analyzed with the TREC. The equipotential contours generated from the voltage scheme arrived at experimentally share the same general feature of shifted region of minimized radial field when compared with results obtained previously by our laboratory through modeling EPIC. Illustrated on both Figure 2a and b are the expected initial postexcitation cyclotron radius from eq 3 for the melittin experiment expressed as a percentage of the inner diameter of the cell.

$$r_{\text{excite}} = \frac{\beta_{\text{dipolar}} V_{p-p} \sqrt{\frac{1}{\text{Sweep Rate}}}}{2dB_{\text{o}}} \tag{3}$$

Where β_{dipolar} is a geometry factor (the closed cylindrical cell (1:1 aspect ratio) value was used;[54] $\beta_{\text{dipolar}} = 0.80818$), V_{p-p} is the applied excitation potential (V), the sweep rate refers to the rate that all excitation frequencies were applied (Hz/s), d is the distance between the trapping electrodes (m), and B_{o} is the magnetic field strength (T). This is only an approximation of the excited ion radius;[28] however, this approximation is adequate for the present discussion. A comparison of the radial electric field over the range of *z*-axis oscillation at 38% cell radius was generated in SIMION and depicted in Figure 3. The equipotential contours in Figure 2 correspond to the voltages applied to the trap plates during this experiment. The radial electric field variation over the *z*-axis is much greater with the common 2.0 V non-TREC conditions. The variation of the radial electric field under TREC conditions is nearly zero over an oscillation amplitude of −10 to 10 mm along the *z*-axis. The trapping well confining the ions in the *z* dimension is superimposed over the radial electric field plot. A reference point of 0.5 V kinetic energy is inscribed within the potential well to illustrate the oscillation amplitude of ions with a liberal amount of kinetic energy following collisional cooling. Certainly the *z*-axis kinetic energy of ion populations in the cell will vary; thus, the depth of penetration into the trapping fields will vary. However, the change in radial electric field over the same *z*-axis oscillation amplitude in a conventional closed cylindrical cell versus the TREC is demonstrated. This is true when considering any region in the central 2/3 of the cell. The voltage modulation scheme placed on the electrodes for this experiment may not be fully optimized. Nonetheless, utilizing the TREC, we have illustrated the ability to minimize the change in radial fields over the *z*-axis oscillation of the ions at their excited cyclotron radius.

The comparison of a single scan spectrum collected with non-TREC and TREC conditions is provided in Figure 4 for melittin $[M + 4H]^{4+}$ species. The extracted time-domain signals are provided, zeroing all points outside the *m/z* range of interest, to show the dramatic contrast in the data obtained with each set of trap plate conditions.[55] In general, additional techniques are used to process FTICR spectra, such as apodization or zero-filling. These processes augment peak shape and other characteristics of the spectrum; therefore, these techniques were not utilized in the data processing. Figure 4a and 4b illustrate spectra in which common 1.1 V conditions were employed. These spectra were acquired varying instrumental parameters including trap plate voltages, accumulation time, and excitation amplitude. The spectra are shown to illustrate that the instrument can achieve respectable performance (mass dependent resolving power in the range of 18 000–278 000), as expected from a 3 T field strength. The difference between these two data sets is the ion population present during data acquisition. 4a used 1 ms ion accumulation time while 4b used 0.5 ms ion accumulation time. Figure 4c shows the transient signal and corresponding mass spectrum

acquired with common 2.0 V conditions applied during detection. Figure 4d shows the transient signal and corresponding mass spectrum under TREC conditions in which the rings were modulated to the following voltages immediately following excitation: 0.2, 1.1, 2.0, 2.4, 2.8 V (voltage profile used in Figures 2 and 3). The spectra shown in Figure 4c and d were acquired under identical experimental conditions, except the voltage profile mentioned above was applied during the detection phase for the TREC spectrum. The dramatic increase in the transient signal length shown in Figure 4d is attributed to the decreased dephasing resulting from minimization of radial electric field differences and magnetron frequencies of the ions. Thus, ions of the same *m/z* ratio (but different *z*-axis KE) possess the same or nearly the same magnetron frequency contribution to the observed cyclotron frequency. Decreased variation in magnetron frequency in an ion population of a given *m/z* promotes coherent motion for a longer duration. Furthermore, when contrasting the common conditions with TREC conditions, we have demonstrated with TREC the ability to acquire long time-domain signals with relatively high trapping potentials. In addition, application of relatively high TREC potentials does not preclude high resolving power, as is normally observed with non-TREC experiments.

For example, the resolving power (fwhm) achieved using the TREC in Figure 4d was 421,000. The resolving power of the non-TREC experiment with the same experimental parameters (Figure 4c) showed 7000. The comparison of the TREC versus common 1.1 V conditions is revealed through Figure 4d and b respectively. In the optimized static experiment, average resolving power over the isotopic envelope was 101 000 (Figure 4b). The resolution was averaged over all of the observable isotopic peaks contained in the isotope envelope for the $[M + 4H]^{4+}$ species. The theoretical resolving power[19] or the highest achievable resolving power for the experiment can be approximated from the expression shown in equation 4.

$$R \cong \frac{f \bullet t}{2} \tag{4}$$

where R is the theoretical resolving power, f is the observed cyclotron frequency, and t is the time duration of the transient signal. The expected theoretical resolving power for this experiment is ~585 000. This indicates that with the TREC modification theoretical resolving power is approached (72% theoretical resolving power). The expected theoretical resolving power for the spectrum in Figure 4b is 210 000, where 48% of theoretical resolving power was achieved. In data sets where the time domain signal has been truncated theoretical resolution is achieved. A transient signal collected over 13 s using the same TREC conditions (see Supplemental Figure 1, Supporting Information) illustrated ~400 000 resolving power with the theoretical resolving power of 423 000 (95% theoretical resolving power). The concept of minimizing radial electric field variation about the excited cyclotron radius of the ions is highly dependent upon how accurately the cyclotron radius and the electric field environment have been matched. Definition of the cyclotron radius is achieved through the excitation event in each ICR experiment. Therefore, gains in S/N and resolution using the TREC are limited by the excitation event.

A 4-fold increase in resolving power is achieved when comparing TREC and optimized non-TREC conditions (common 1.1 V). An important observation of the TREC spectrum is that the frequency does not drift with time over this long transient signal as noted in conventional ICR cells[56,57] (Supplemental Figure 2, Supporting Information). An inset showing a magnified view of the most abundant isotope peak (Figure 4) of the melittin $[M + 4H]^{4+}$ species reveals little asymmetry in the peak shape for the TREC spectrum as compared with the non-TREC spectra. The “tailing” observed in the peaks shown for non-TREC conditions,

(Figure 4a and b) indicates a shift in frequency over the data acquisition period. Frequency stability over the data acquisition time period is also thought to be responsible for the observed increase in performance using the TREC. A comparison of the S/N ratio in the spectra presented in Figure 4 shows a 10-fold improvement in the TREC over optimized non-TREC spectra.

Improved S/N resultant from excitation to large cyclotron radii is possible because the signal intensity in FTICR is proportional to the proximity of ions to the detection electrodes. Sensitivity is fundamentally related to S/N. Investigation of the S/N in both the static and TREC conditions provides an important comparison, since the only experimental variable altered was the trapping voltage during detection. Quantification of the gain in S/N using TREC over non-TREC conditions is presented in Figure 5. SIMION was used to predict four voltage profiles for performance enhancement at the specified postexcitation cyclotron radius. The criterion used to select these voltage schemes was the electric field environment at or near the axial region of the excited cyclotron radius predicted by eq 3. A direct comparison, the change in S/N with the TREC over non-TREC conditions, is depicted in Figure 5. Overall, approximately a 10-fold gain in S/N is achieved with the TREC over common 2.0 V conditions in the range of radii studied (35%–65% cell radius).

The ability to tune the electrical potentials for decreased radial electric field variation over the axial oscillation is an important feature of the TREC which enables the performance improvements demonstrated. This tunability is experimentally represented in Figure 6. These data were generated using single frequency excitation of bradykinin $[M + 2H]^{2+}$ with the excitation amplitude being varied incrementally. Each data point is a signal average of ten consecutive scans. Data acquisition was decreased to 0.4 s for each scan, as high resolution was not of primary importance to the results. The total ion intensity (absolute) was summed over the isotopic envelope, with a threshold of three times the S/N. Initial postexcitation cyclotron radii were generated using the single frequency version of eq 3. Using single frequency excitation, the approximation this equation provides appears to hold; at the boundary of the cell (100% cell radius) the signal plummets to zero intensity. The three TREC profiles, TREC 1, TREC 2, and TREC 3, have a different postexcitation radius for which enhancement in ion intensity appears the strongest, ~62, 70, and ~52% cell radius, respectively. An interesting observation in these data is that at low cyclotron radii, ~39% cell radius and smaller, the common 2 V condition shows higher ion intensity. This can be predicted by considering the equipotential contours produced with common 2 V potentials placed on all of the rings. The region in the cell where the radial electric field variation is the smallest is centered about 0% cell radius. Using the TREC voltage profiles designed for this experiment actually would create a radially inward directed electric field component in which the magnitude would increase as 0% cell radius was approached.

This experiment also reveals the ability of the TREC to provide enhancement on the throughput time scale necessary for LC-MS analysis. Figures 6b and c are shown for comparison at maximum ion intensity for both common 2.0 V and the TREC 3 conditions. The damping rate in the transient signals for both experiments is dramatically different. This is apparent in the spectral quality, considering resolution and S/N of the spectra in Figure 6. The high duty-cycle demand that LC-MS places on an instrument make it difficult to achieve high performance and high throughput simultaneously, so the instrument performance enhancements the TREC provides make it valuable to this type of analysis.

It must be mentioned that although the current TREC design (Figure 1), which consists of five ring electrodes, allows modulation of radial fields near the expected postexcitation cyclotron radius, a design containing more than five independently controlled electrodes would impart better definition and control over the potentials within the trapping region. The

current TREC design is focused on producing electric fields ideally suited for detection, and we have not addressed in the design its susceptibility to *z*-axis ejection during excitation. However, the TREC design is compatible with the Infinity Cell[45] concept or a similar approach where excitation has been coupled to the segmented trap plates. Integrating the TREC concept with excitation coupled to the trapping ring electrodes would address *z*-axis ejection[46] and linearize the excitation profile (Supplemental Figures 3 and 4, Supporting Information), while retaining the ability to moderate the radial electric fields during detection.

CONCLUSION

Through the theory, development, and implementation of the TREC, performance of FTICR-MS was greatly increased. The TREC is one novel component in an original FTICR mass spectrometer being developed by our laboratory. The resolution was increased by greater than a factor of 4 over optimized non-TREC conditions (common 1.1 V) and potentially can be further optimized for additional gain. The S/N was shown to be increased by a factor of 10 over common conditions. The mechanism for the gain in performance has been shown to occur by mitigating the change in radial electric field in the region of the postexcitation cyclotron motion of the ions. In addition, it was shown that tuning the radius for which the greatest enhancement in signal is applied (~50–70% cell radius) is possible with the TREC, simply by altering the voltage profile applied after excitation of ion cyclotron motion. This technology is flexible and can be implemented on commercial instruments. It is expected that the enhancements provided with the new TREC technology will be scalable to the magnetic field utilized. Convolving the TREC with the concept of coupled RF excitation to the trap plate segments will provide an ICR cell which effectively addresses linearization of excitation potential and reduction in the change in radial electric field over ion oscillation. The TREC also may provide a unique opportunity to study the effects of space charge and image charge with a decreased perturbation due to coherent ion motion via decreased difference in magnetron frequency.

Supplementary Material

Refer to Web version on PubMed Central for supplementary material.

Acknowledgments

We acknowledge Alan Marshall and his group at the National High Magnetic Field Laboratory for the use of the MIDAS data station. This material is based upon work supported by the Directorate of Biological Sciences, National Science Foundation under Grant No. 0352451; Murdock Charitable Trust; and Office of Science (BER), U.S. Department of Energy, Grant No. DE-FG02-04ER63924.

References

1. Comisarow MB, Marshall AG. Chem. Phys. Lett 1974;25:282–283.
2. Henry KD, Williams ER, Wang BH, McLafferty FW, Shabanowitz J, Hunt DF. Proc. Natl. Acad. Sci. U.S.A 1989;86:9075–9078. [PubMed: 2594751]
3. Kelleher NL, Nicewonger RB, Begley TP, McLafferty FW. J. Biol. Chem 1997;272:32215–32220. [PubMed: 9405424]
4. Olsen JV, Mann M. Proc. Natl. Acad. Sci. U.S.A 2004;101:13417–13422. [PubMed: 15347803]
5. Brown SC, Kruppa G, Dasseux J-L. Mass Spectrom. Rev 2005;24:223–231. [PubMed: 15389859]
6. Marshall AG, Rodgers RP. Acc. Chem. Res 2004;37:53–59. [PubMed: 14730994]
7. Rodgers RP, Schaub TM, Marshall AG. Anal. Chem 2005;77:20A–27A. [PubMed: 15623274]
8. Bossio Robert E, Marshall Alan G. Anal. Chem 2002;74:1674–1679. [PubMed: 12033259]

9. Lipton MS, Pasa-Tolic L, Anderson GA, Anderson DJ, Auberry DL, Battista JR, Daly MJ, Fredrickson J, Hixson KK, Kostandarithes H, Masselon C, Markillie LM, Moore RJ, Romine MF, Shen Y, Stritmatter E, Tolic N, Udseth HR, Venkateswaran A, Wong K-K, Zhao R, Smith RD. Proc. Natl. Acad. Sci. U.S.A 2002;99:11049–11054. [PubMed: 12177431]
10. Tang X, Munske GR, Siems WF, Bruce JE. Anal. Chem 2005;77:311–318. [PubMed: 15623310]
11. He F, Emmett MR, Hakansson K, Hendrickson CL, Marshall AG. J. Proteome Res 2004;3:61–67. [PubMed: 14998164]
12. Goodlett DR, Bruce JE, Anderson GA, Rist B, Pasa-Tolic L, Fiehn O, Smith RD, Aebersold R. Anal. Chem 2000;72:1112–1118. [PubMed: 10740847]
13. Spengler B. J. Am. Soc. Mass. Spectrom 2004;15:703–714. [PubMed: 15121200]
14. Dehmelt H. RvMP 1990;62:525–530.
15. McIver RT Jr. Rev. Sci. Instrum 1970;41:555–558.
16. Penning FM. Ned. Tijdschr. Natuurkd 1936;3:141–154.
17. Marshall AG, Guan S. Phys. Scr., T 1995;T59:155–164.
18. Peurrung AJ, Kouzes RT. Int. J. Mass Spectrom. Ion Processes 1995;145:139–153.
19. Marshall AG, Comisarow MB, Parisod G. J. Chem. Phys 1979;71:4434–4444.
20. Peurrung AJ, Kouzes RT. Phys. Rev. E: Stat. Phys., Plasmas, Fluids 1994;49:4362–4368.
21. Capron MA, Haskin SS, Hanson CD. J. Iowa Acad. Sci 1992;99:1–6.
22. Hanson CD, Castro ME, Kerley EL, Russell DH. Anal. Chem 1990;62:520–526.
23. Mitchell DW, Hearn BA, DeLong SE. Int. J. Mass Spectrom. Ion Processes 1993;125:95–126.
24. Francl TJ, Sherman MG, Hunter RL, Locke MJ, Bowers WD, McIver RT Jr. Int. J. Mass Spectrom. Ion Processes 1983;54:189–199.
25. Mitchell DW, Smith RD. J. Mass Spectrom 1996;31:771–790.
26. Wong RL, Amster IJ. Int. J. Mass spectrom 2007;265:99–105. [PubMed: 19562102]
27. Solouki T, Emmett MR, Guan S, Marshall AG. Anal. Chem 1997;69:1163–1168. [PubMed: 9075406]
28. Marshall AG, Hendrickson CL, Jackson GS. Mass Spectrom. Rev 1998;17:1–35. [PubMed: 9768511]
29. Jeffries JB, Barlow SE, Dunn GH. Int. J. Mass Spectrom. Ion Processes 1983;54:169–187.
30. Vartanian VH, Laude DA. Int. J. Mass Spectrom 1998;178:173–186.
31. Bruce JE, Anderson GA, Lin C-Y, Gorshkov M, Rockwood AL, Smith RD. J. Mass Spectrom 2000;35:85–94. [PubMed: 10633238]
32. Brustkern, AM.; Rempel, DL.; Gross, ML. Abstracts of posters. 55th ASMS Conference on Mass Spectrometry and Allied Topics; June 3–7, 2007; Indianapolis, IN. Santa Fe, NM: American Society for Mass Spectrometry; 2007. MP 056
33. Gooden JK, Rempel DL, Gross ML. J. Am. Soc. Mass Spectrom 2004;15:1109–1115. [PubMed: 15234369]
34. Kanawati B, Wanczek KP. Rev. Sci. Instrum 2007;78:074102/07410–074102/074108. [PubMed: 17672776]
35. Tolmachev AV, Robinson EW, Wu S, Kang H, Lourette NM, Pasa-Tolic L, Smith RD. J. Am. Soc. Mass Spectrom 2008;19:586–597. [PubMed: 18296061]
36. Vartanian VH, Hadjarab F, Laude DA. Int. J. Mass Spectrom. Ion Processes 1995;151:175–187.
37. Guan S, Marshall AG. Int. J. Mass Spectrom. Ion Processes 1995;146/147:261–296.
38. Rempel DL, Ledford EB Jr, Huang SK, Gross ML. Anal. Chem 1987;59:2527–2532. [PubMed: 3688441]
39. Yin WW, Wang M, Marshall AG, Ledford EB Jr. J. Am. Soc. Mass. Spectrom 1992;3:188–197.
40. Gabrielse G, Haarsma L, Rolston SL. Int. J. Mass Spectrom. Ion Processes 1989;88:319–332.
41. Gabrielse G, MacKintosh FC. Int. J. Mass Spectrom. Ion Processes 1984;57:1–17.
42. Wang M, Marshall AG. Anal. Chem 1989;61:1288–1293. [PubMed: 2757208]
43. Naito Y, Fujiwara M, Inoue M. Int. J. Mass Spectrom. Ion Processes 1992;120:179–192.
44. Beu SC, Laude DA Jr. Anal. Chem 1992;64:177–180.

45. Caravatti P, Allemann M. Org. Mass Spectrom 1991;26:514–518.
46. Van der Hart WJ, Van de Guchte WJ. Int. J. Mass Spectrom. Ion Processes 1988;82:17–31.
47. Kaiser NK, Bruce JE. Anal. Chem 2005;77:5973–5981. [PubMed: 16159130]
48. Kaiser NK, Bruce JE. Int. J. Mass Spectrom 2007;265:271–280.
49. Kaiser NK, Weisbrod CR, Webb BN, Bruce JE. J. Am. Soc. Mass. Spectrom 2008;19:467–478. [PubMed: 18262433]
50. Senko MW, Canterbury JD, Guan S, Marshall AG. Rapid Commun. Mass Spectrom 1996;10:1839–1844. [PubMed: 8953786]
51. Kaiser NK, et al. 2008 Manuscript in preparation.
52. Wu S, Zhang K, Kaiser NK, Bruce JE, Prior DC, Anderson GA. J. Am. Soc. Mass. Spectrom 2006;17:772–779. [PubMed: 16603374]
53. Anderson, GA.; Bruce, JE.; Smith, RD. ICR-2LS, version 2.18. Richland, WA: Data Processing Software; 2004.
54. Jackson GS, Canterbury JD, Guan S, Marshall AG. J. Am. Soc. Mass. Spectrom 1997;8:283–293.
55. Bresson JA, Anderson GA, Bruce JE, Smith RD. J. Am. Soc. Mass. Spectrom 1998;9:799–804.
56. Bruce JE, Anderson GA, Hofstadler SA, Winger BE, Smith RD. Rapid Commun. Mass Spectrom 1993;7:700–703.
57. Guan S, Wahl MC, Marshall AG. Anal. Chem 1993;65:3647–3653. [PubMed: 8311249]

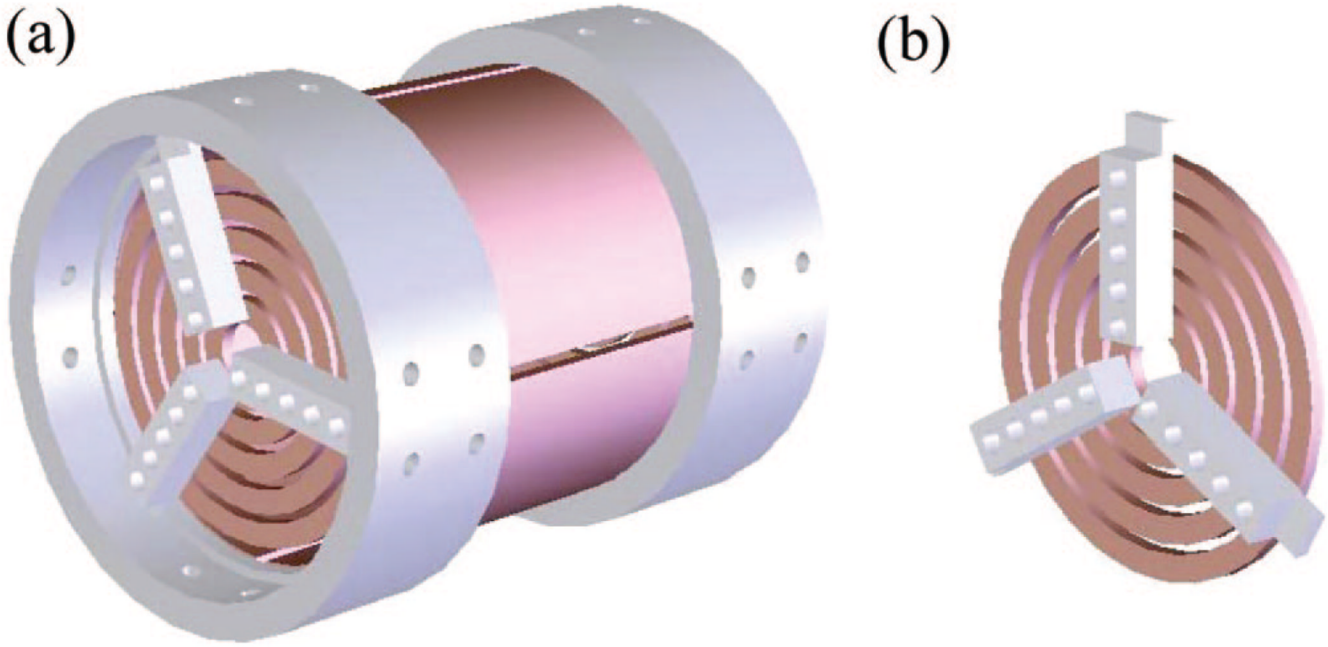

Figure 1.
(a) Conceptual representation of the TREC. (b) Conceptual representation of a single TREC trap plate (magnified view).

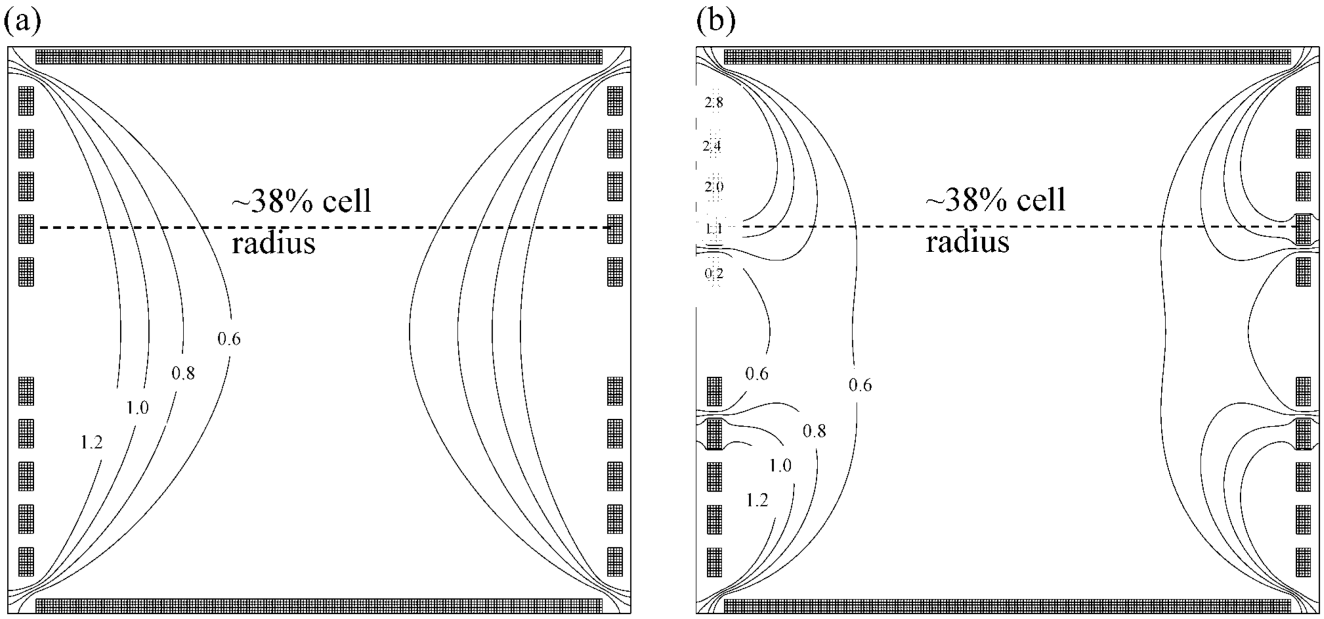

Figure 2.

Equipotential contour plots are shown for (a) common 2.0 V trapping conditions and (b) the TREC trapping conditions. The voltages for the modulated (TREC) trapping conditions with increasing electrode radius are 0.2, 1.1, 2.0, 2.4, and 2.8 V respectively, as shown on the rings. A dashed line through the cell located at 38% cell radius is depicted.

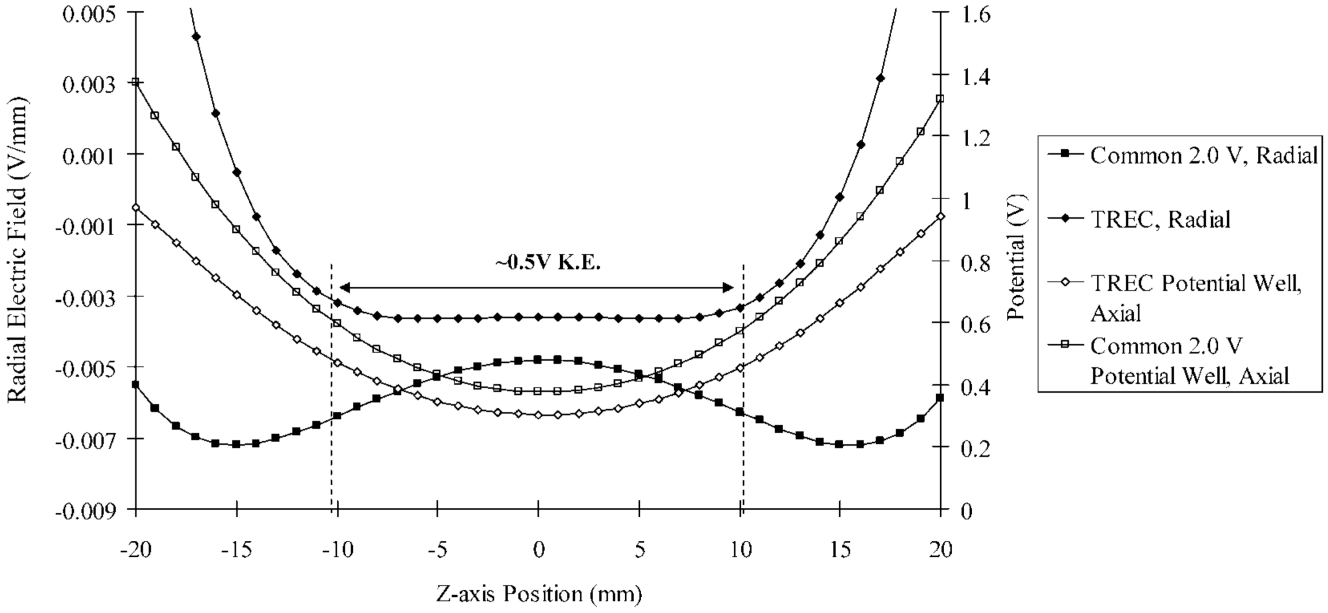

Figure 3.

Radial electric field plots generated at 38% cell radius for both common 2.0 V trapping conditions and the TREC modulated conditions. A trapping potential well generated from the TREC conditions is overlaid to provide perspective.

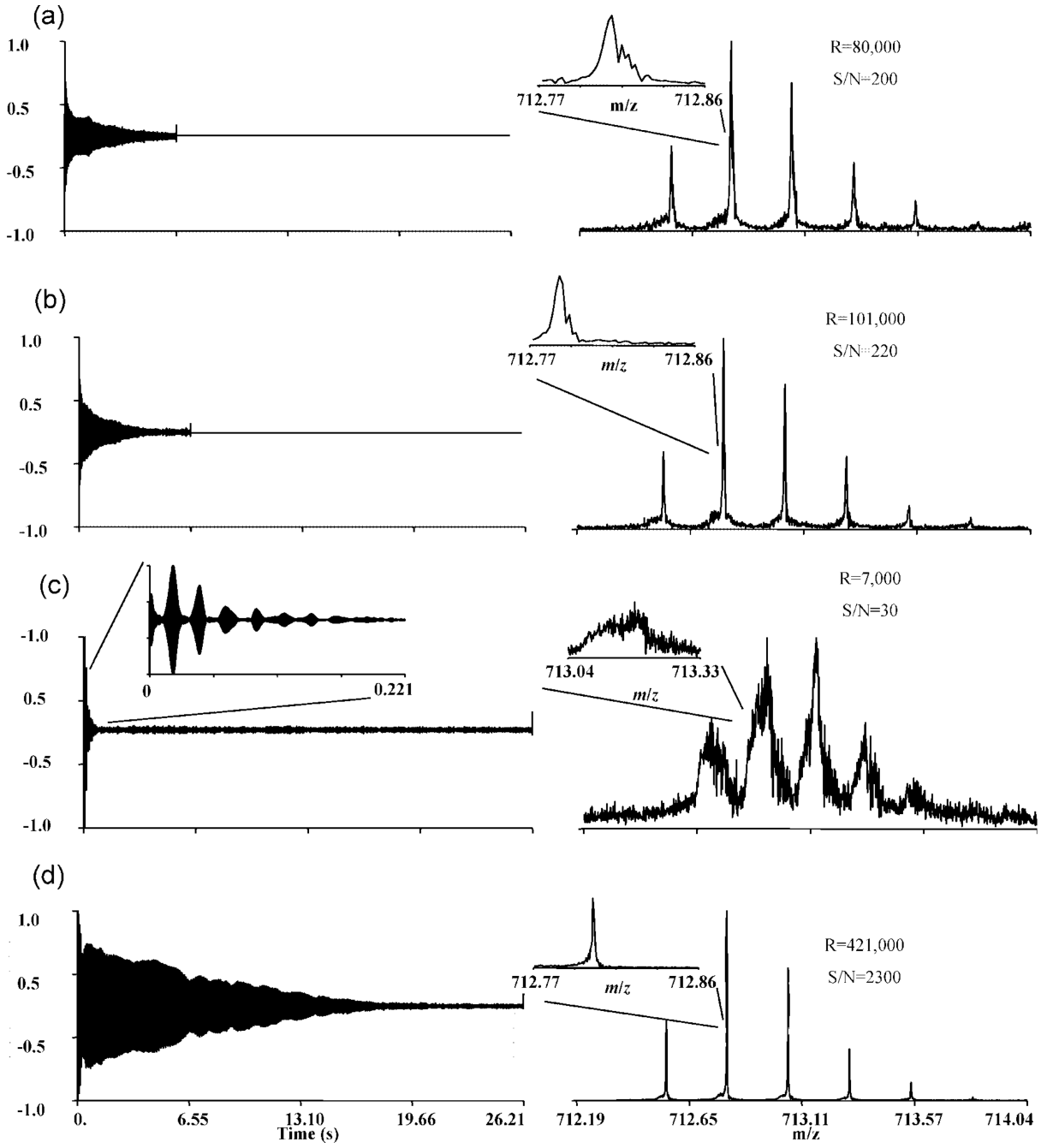

Figure 4.

Comparison of melittin $[M + 4H]^{4+}$ spectra acquired with static and the TREC conditions. (a) Spectrum collected with static 1.1 V conditions with increased ion population. (b) Spectrum collected with optimized common 1.1 V conditions with a decreased ion population. (c) Spectrum collected with common 2.0 V conditions. (d) Spectrum collected using the TREC, modulating the voltages only during the detection phase. (Insets) Peak shape of the most abundant isotopic peak in each case.

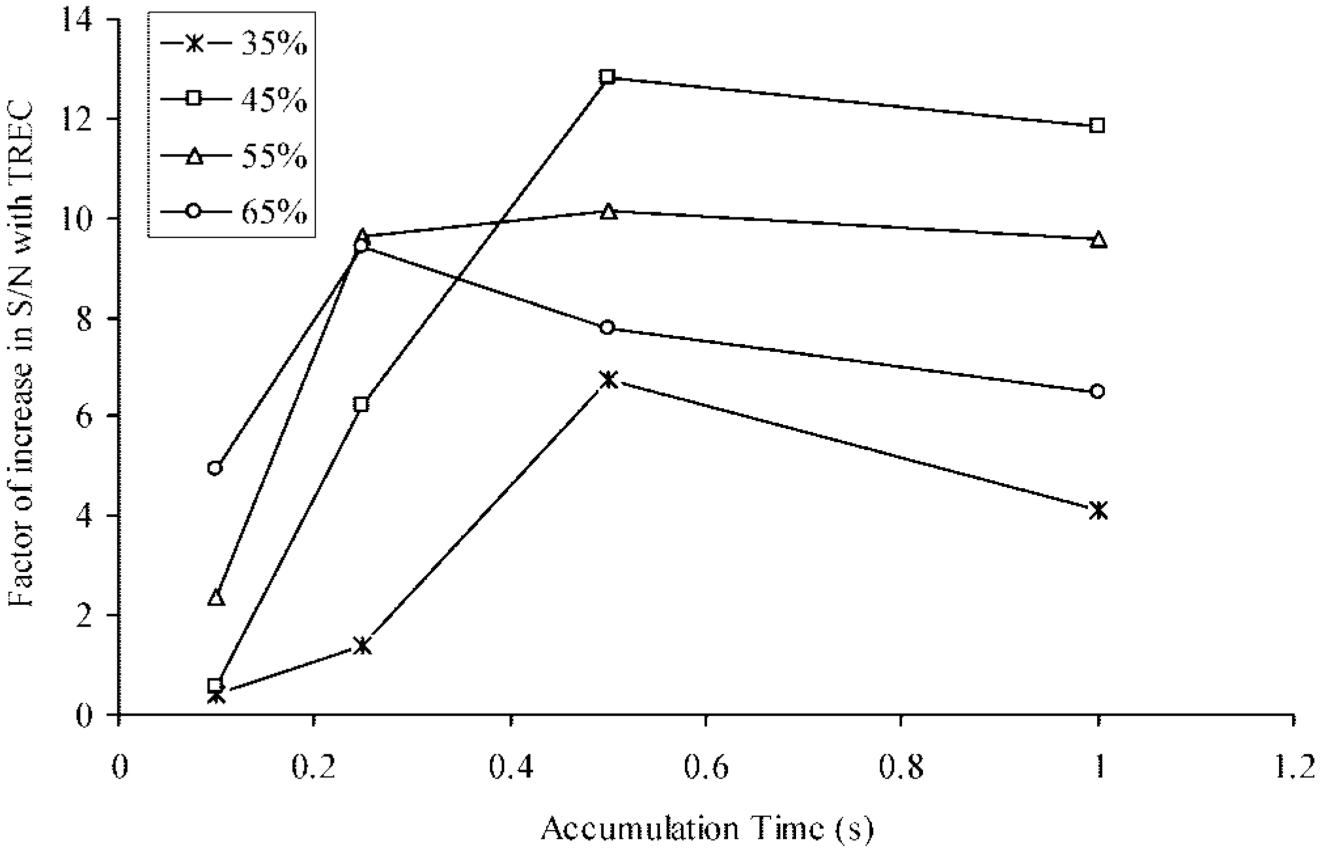

Figure 5.
Change in S/N of the TREC over common 2.0 V conditions is shown. A 10-fold increase in S/N is achieved using the TREC technology over the radii studied (35%–65% cell radius).

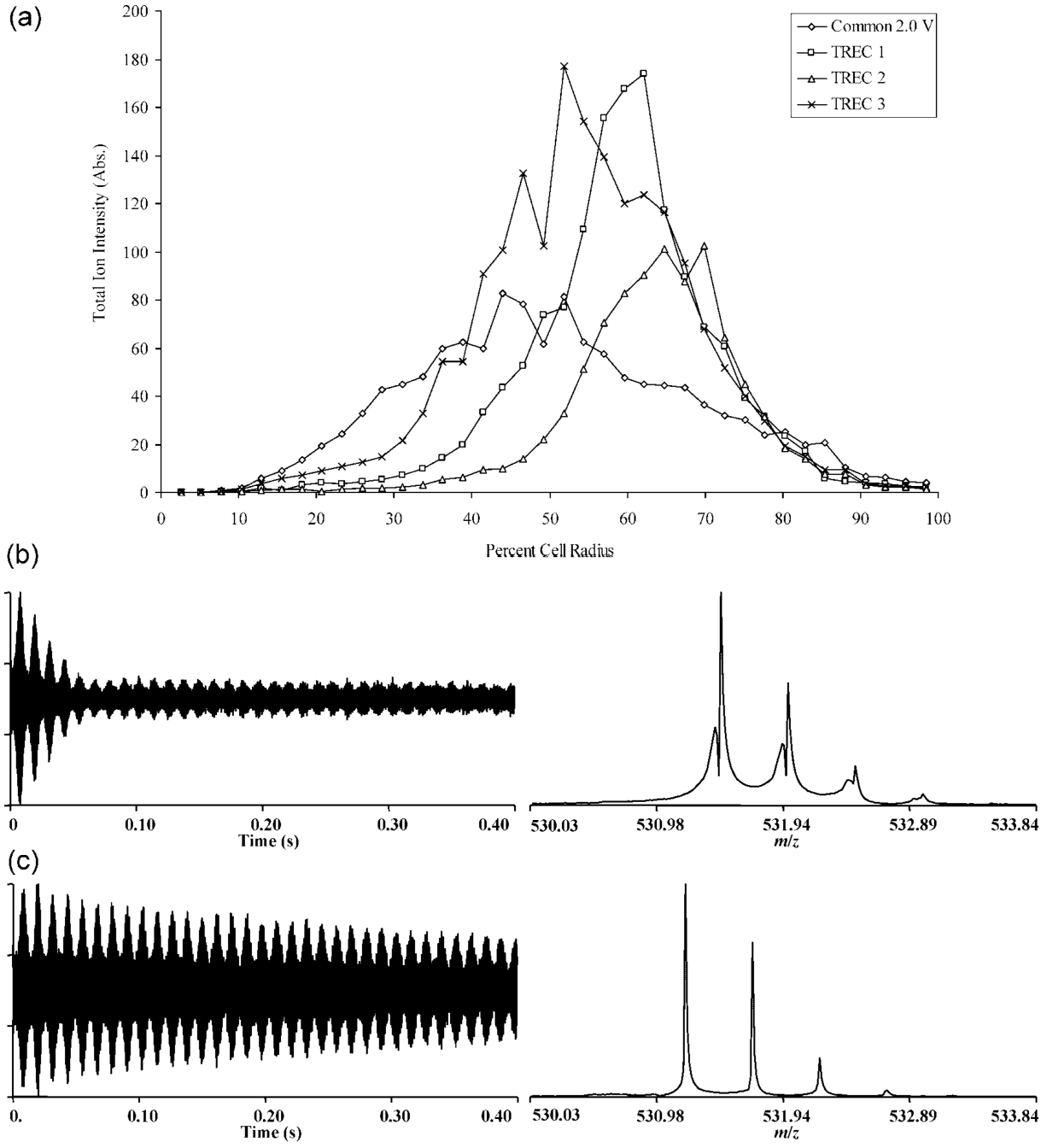

Figure 6.

(a) Total ion intensity (absolute) of the bradykinin $[M+2H]^{2+}$ isotopic envelope vs % cell radius for common 2.0 V trapping compared to a variety of TREC voltage profiles. (b), Representative spectrum using single frequency excitation of bradykinin $[M + 2H]^{2+}$ for common 2.0 V conditions. (c) Representative spectrum using single frequency excitation of bradykinin $[M + 2H]^{2+}$ for the TREC 3 conditions (1.2, 1.4, 1.6, 2.0, 2.4 V).